ICEM12- 12th International Conference on Experimental Mechanics
29 August - 2 September, 2004 Politecnico di Bari, Italy

The digital image correlation technique as full field strain technique on biaxial loaded composites using cruciform specimens

Smits A.[a], Van Hemelrijck D.[a], Philippidis T.[b]

[a] *Department of Mechanics of Materials and Constructions, Vrije Universiteit Brussel /Free University of Brussels(VUB), Pleinlaan 2, 1050 Brussels, BELGIUM, arwen.smits@vub.ac.be*
[b] *Department of Mechanical Engineering & Aeronautics, University of Patras, P.O. Box 1401, Patras 265 00, Greece*

ABSTRACT
Experimental investigation of fibre reinforced composites was predominantly performed using uni-axially loaded specimens. However, composites are often subjected to complex multi-axial loadings in service and consequently, experimental investigation should consider bi-axial tests. For this reason a bi-axial testing facility for planar cruciform specimens was developed at the department of Mechanics of Materials and Constructions of the Free University of Brussels. A valid and useful bi-axial test avoids failure in the uni-axially loaded arms and gives a large region of uniform strain in the bi-axially loaded zone, conditions which are not easily obtained simultaneously. To be able to select a suitable geometry, finite element simulations investigating the influence of various parameters in combination with experiments on different geometries using the digital image correlation technique for full field strain measurement were performed.

1. INTRODUCTION
All too often, mechanical testing of fibre reinforced composites was (and still is) limited to uni-axially loaded specimens. In service, fibre reinforced composites are hardly ever loaded in one direction. Since the material properties are optimized for the primary load, even small secondary loads can lead to failure when they coincide with a weakness in the material. Experimental investigation of these materials should approximate real life behaviour as much as possible. In an attempt to achieve this goal bi-axial tests can be considered [1]. When bi-axial loads are applied, it is usually by superimposing a torsion load on tubular specimens subjected to tension or compression [2, 3]. Real construction components in fibre reinforced composite materials however, are often made in the form of flat or gently curved panels. Moreover, thin-walled tubes are not easy to fabricate and obtaining a perfect alignment and load introduction is not straightforward. Furthermore failure often occurs at the edge due to stress concentrations or local buckling [4, 5]. For this reason a bi-axial testing facility for planar cruciform specimens (Fig. 1) was developed at the Free University of Brussels.

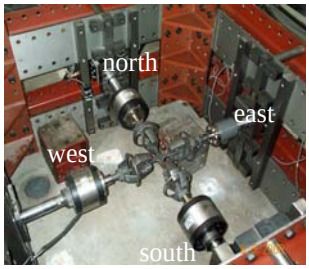

Fig. 1. Bi-axial test bench for flat cruciform specimens.

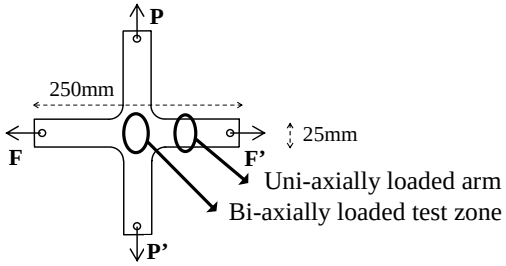

Fig. 2. Cruciform geometry with identification of forces.

2. PLANAR BI-AXIAL TESTING DEVICE

A bi-axial tension test bench for planar cruciform specimens with a maximum capacity of 100 kN is used. A successful bi-axial loading test satisfies two criteria: a test zone with a uniform bi-axial stress distribution should be obtained, and specimen failure must occur within this bi-axially loaded test zone —not in the uni-axially loaded arms. To fulfil the uniformity requirement, the force P has to be equal and collinear to the P' and the force F equal and collinear to F' (Fig. 2). In addition P & P' has to be perpendicular to F & F'.

In order to maintain the co linearity —i.e., avoid bending moments which cause non-uniform stress distribution in the bi-axially loaded zone— it is desirable that the centre of the specimen does not undergo any displacement. A simple arrangement where two ends of the cruciform specimen are held fixed while the opposite ends are loaded, is unsatisfactory in this respect. Instead, four servo-hydraulic cylinders are used, with a control unit to explicitly keep the forces collinear (Fig. 3). As no cylinders with hydrostatic bearing were used, the test frame is limited to loading in tension. Failure or slip in one arm of the specimen will result in sudden radial forces which could seriously damage the servo-hydraulic cylinders and load cells. To prevent this, hinges were used to connect the specimen with the cylinders and to connect the cylinders to the test frame. Using four hinges for each loading direction results in an unstable situation in compression and consequently only tests in tension can be performed. In an ideal situation the forces are as shown in Fig. 4a and no displacement of the centre point of the specimen is observed. If a displacement occurs (for instance in the Y-direction) an imbalance arises in the forces, as shown in Fig. 4b (a component F_y is added).

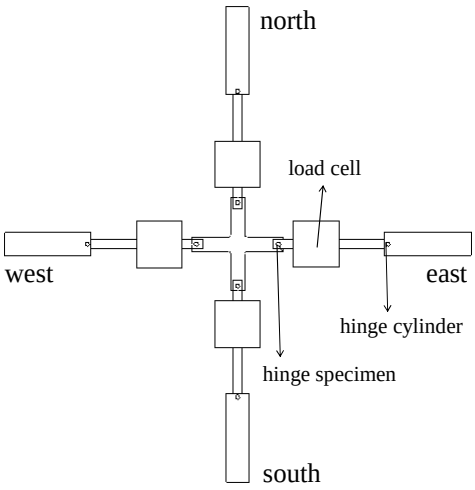

Fig. 3. Schematic illustration of the bi-axial test set-up.

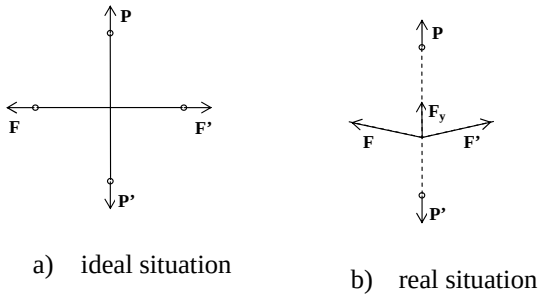

Fig. 4. Forces on the cruciform specimen.

From the force equilibrium in the Y-direction we obtain:

$$P + F_y = P' \tag{1}$$

Due to the displacement, the absolute value of the force |P| is no longer equal to |P'|. However as four load cells are used, it is possible to measure this small difference in loads during load controlled tests. In fact, this measured difference is used as a control signal in this direction.

The same is done in the perpendicular direction. Thus, active control is used to maintain the co linearity of the applied loads.

3. CRUCIFORM SPECIMEN DESIGN

It has proven extremely difficult to develop a cruciform test specimen that simultaneously fulfils the following conditions: (i) there has to be a uniform strain state in the bi-axially loaded test zone, (ii) failure has to occur in the bi-axially loaded test zone and not in the uni-axially loaded arms, and (iii) the results should be repeatable [3, 5]. To investigate the influence of parameters like (i) the rounding radius at the intersection of the arms, (ii) the thickness of the bi-axial loaded test zone in relation to the thickness of the arms and (iii) the geometry of the bi-axial loaded test zone, finite element simulations were performed simulating with the complete lay-up of the composite material. Afterwards, the numerical results were compared with experimental results obtained on selected cruciform geometries using a digital image correlation technique for full field strain measurement. Strain gauges were also used as a reference.

3.1 Finite element simulations

The finite element simulations were performed with the commercial software *Ansys* inc. *7.1* using element type *shell 99*. This element has six degrees of freedom at each node: three translations and three rotations. It is defined by eight nodes, the average or corner layer thicknesses, the layer material direction angles and the orthotropic material properties. It may be used for layered applications of a structural shell model and allows up to 250 layers. Strains and stresses are computed at the mid thickness of each layer. Due to symmetry, only one quarter of the cruciform geometry of each simulation is shown. The bi-axially loaded test zone was zoomed in, but the finite element calculation was performed with much longer arms. Fig. 6 shows the finite element results of the first and second principal strains for three geometries A, B and C modelled as glass fibre reinforced epoxy with a $[(+45°\ -45°\ 0°)_4(+45°\text{-}45°)]$-lay-up (zone 2 on Fig. 6 with lay-up 2 on Fig. 5). This material with this specific lay-up is often used for wind turbine rotor blades, as they are globally submitted to bending combined with torsion. The $(\pm 45°)$-layers serve to carry torsion and the $0°$-layers to carry bending. The load ratio between the x- and y-directions was chosen equal to the strength ratio of both arms i.e. 553,8 MPa/143,9MPa=3.85/1 (Table 1). The $(\pm 45°)$-layers have a thickness of 0.611mm; the $0°$-layers of 0.88mm. This gives a total thickness of 6.57mm for zone 2 and 3.59mm for zone 3. The end-tabs are 2.5mm in thickness each.

Table 1. Uni-axial properties of the tested glass fibre reinforced epoxy composite.

property	dimensions	average	stdev
longitudinal stiffness modulus, E_x	(GPa)	28,70	1,01
transverse stiffness modulus, E_y	(GPa)	15,15	0,78
Poisson's ratio, ν_{xy}	(-)	0,47	0,05
Poisson's ratio, ν_{yx}	(-)	0,28	0,06
longitudinal tensile strength, X	(MPa)	553,8	18,7
longitudinal tensile failure strain, ε_x	(%)	2,45	0,09
transverse tensile strength, Y	(MPa)	143,9	3,0
transverse tensile failure strain, ε_y	(%)	2,90	0,17

End-tabs were glued on the arms of all the specimens (zone 1). In the middle of geometries B and C a layer of (0° +45° -45°) was milled away at each side of the specimen (zone 3). The applied forces simulated were F_x/F_y = 46.2kN/12kN.

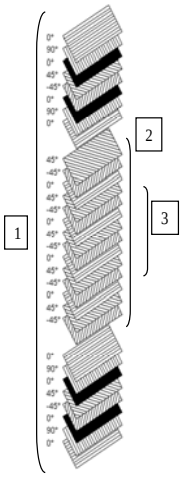

Fig. 5. Lay-up.

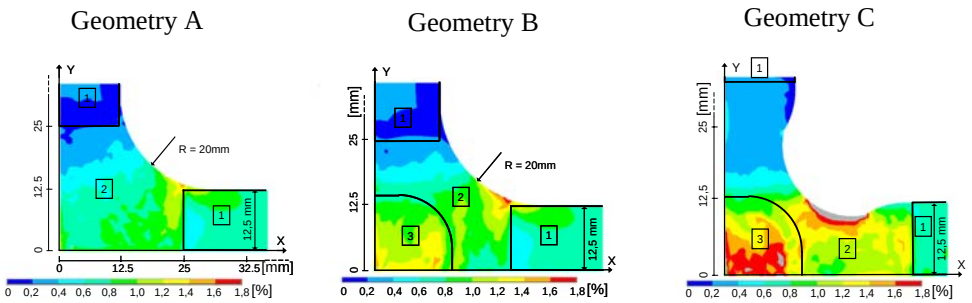

Fig. 6. Orthotropic finite element results for three cruciform specimens. First principal strains are shown.

For geometry A, the first principal strains in the x-direction just beyond the end-tabs are higher than in the end-tabs, but are lower in the neighbourhood of the centre of the specimen. This is due to the enlargement of the area taking the load in this region. Consequently, failure of the specimen will occur close to the end-tabs. In order to increase the strains and the likelihood of failure in the bi-axially loaded zone, a reduction of the thickness and/or changing the rounding radius at the intersection of two perpendicular arms is necessary. In geometry B the first suggestion is shown. The strain results are improved; for this kind of geometry failure can occur at the middle of the specimen. If we use a combination of both suggestions, as shown in geometry C, even higher strains are obtained in the bi-axial loaded zone.

3.2 Experiments on cruciform specimens using strain gauges

The experimental results for the three tested geometries A, B and C submitted to a load ratio F_x/F_y of 3,85/1 are shown in Table 2. Each value is an average of at least four experiments. Strain measurements were obtained in x- and y- direction by using rosette strain gauges of 6mm length glued in the centre of each specimen. The failure loads and failure strains were measured in both perpendicular directions. With these strain gauges only one average value of the strains is obtained for the two directions. No information regarding the uniformity of the strains in the bi-axially loaded test zone is captured. For that purpose full field strain measurement techniques are needed, as elaborated in the next paragraph. Failure stresses could not be calculated from the failure forces, since the load-bearing area is ill-defined with a cruciform geometry. Therefore, the failure stresses were calculated from the experimentally obtained failure strains using the stiffness moduli and Poisson's ratios measured on uni-axially loaded specimens (Table 1). The formulas giving the strains ε_x in the x-direction and ε_y in the y-direction in function of the occurring stresses σ_x and σ_y are:

$$\varepsilon_x = \sigma_x/E_x - \nu_{xy}\sigma_y/E_y \qquad \varepsilon_y = -\nu_{yx}\sigma_x/E_x + \sigma_y/E_y \tag{2}$$

Conversely, stresses can be calculated from the measured strains:

$$\sigma_y = (\varepsilon_y + \nu_{yx}\varepsilon_x)\, E_y/(1- \nu_{yx}\nu_{xy}) \tag{3}$$

$$\sigma_x = (\varepsilon_x + \nu_{xy}\sigma_y/E_y)E_x = (\varepsilon_x + \nu_{xy}(\varepsilon_y + \nu_{yx}\varepsilon_x)/(1- \nu_{yx}\nu_{xy}))E_x$$

The results of the obtained failure loads, failure strains and calculated failure stresses are shown in Table 2 for the tested load ratio 3.85/1.

Table 2. Experimental results of three cruciform specimens.

	[kN]		[%]		[MPa]	
	F_x	F_y	ε_x	ε_y	σ_x	σ_y
geometry A	63,2	16,5	1,35	-0,56	395	14
geometry B	60,5	15,8	1,52	-0,66	442	13
geometry C	47,9	12,4	1,68	-0,47	516	56

The highest failure strains are obtained for geometry C, indicating this geometry is the most promising one. Pictures recorded immediately prior to (upper frame) and during failure (lower frame) are shown in Fig. 7 for each of the three geometries. For geometry A, failure of the specimen didn't occur in the bi-axial loaded test zone, whereas in geometries B and C it did. The high values for the experimentally obtained failure strains indicate that the strain concentrations at the rounding between the two perpendicular arms in geometry C —seen in the finite element simulations— do not cause early failure of the specimen.

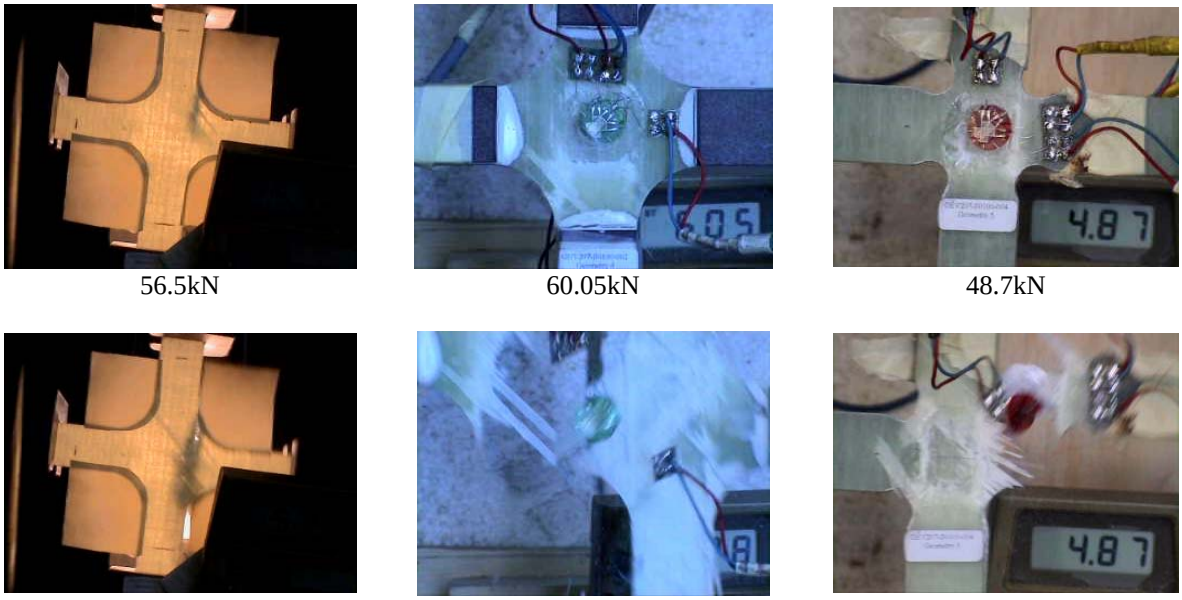

56.5kN | 60.05kN | 48.7kN

failure, 57.4kN | failure, 60.08kN | failure, 48.7kN

Geometry A | Geometry B | Geometry C

Fig. 7. Failure of cruciform specimens.

For all geometries, failure starts at the rounding radius between the two arms —not from the middle of the specimen— but for geometries B and C the whole bi-axially loaded test zone is damaged afterwards. From these results geometry C was selected to use for further experimental investigation at different load ratio's using the digital image correlation technique.

3.3 Comparison between finite element results and results obtained with the digital image correlation technique

Digital image correlation is a full field measurement technique that detects deformations using image processing. Once the deformations of a speckle pattern applied to the specimen

have been measured, the strain distribution in the material can be calculated. This allows the uniformity of strains in a certain zone to be judged. The fundamental principle of this technique is based on the correspondence, for a large number of distinguishable small areas —known as macro image facets— between the distribution of grey scale values in the undeformed state and the distribution of grey scale values of the same area in the deformed state. The only limitation is that each facet must contain grey value gradients in both coordinate directions. This technique can allocate coordinates to every pixel in digital images. By tracking the facets in each successive image with sub-pixel accuracy, relative displacements are obtained and the resulting strains can be derived [6, 7]. In Fig. 8 the strain results obtained with the digital image correlation technique are compared with the finite element simulation results for geometry B. The pictures were taken immediately prior to failure of the specimen at a load of F_x/F_y=61.6kN/16kN.

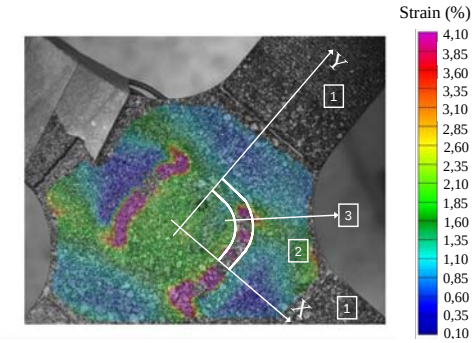

a) First principal strain obtained with the DICT

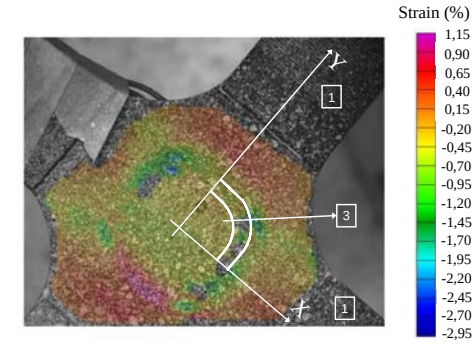

b) Second principal strain obtained with the DICT

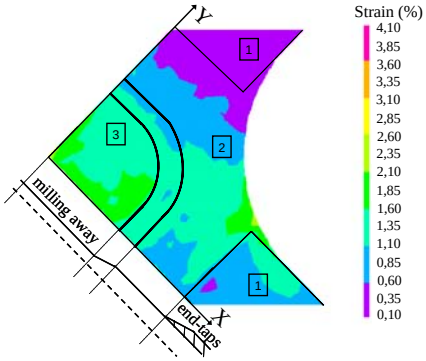

a) First principal strain obtained with finite element simulations

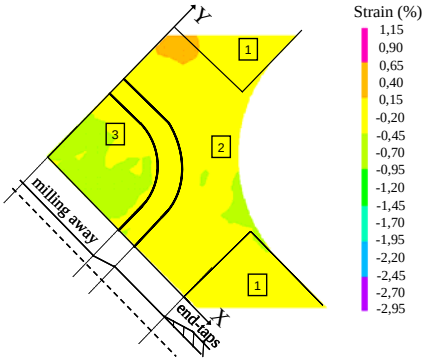

b) Second principal strain obtained with finite element simulations

Fig. 8. Comparison between results of the digital image correlation technique and finite element simulations.

The results of the digital image correlation and the finite element simulations are substantially in agreement, both for the first and second principal strains. Only in the transition zone between the full thickness and the milled area, high strains are observed with the digital image correlation technique but not in the finite element simulations. This may be due to the fact that only one camera was used, able to detect only in plane displacements on flat areas accurately. Also the measured values in the x- and y-direction in the centre of the specimen with strain gages of 1.52% in the x-direction and -0.66% in the y-direction are comparable with the values obtained with the digital image correlation technique.

5. BIAXIAL FAILURE ENVELOPE

The combination of finite element simulations and experimental results from strain gages and from the digital image correlation technique, led to the decision to select geometry C for further investigation. On this geometry tests were performed with different load ratios to be able to set up the biaxial failure envelope. Fig. 9 shows the biaxial failure envelopes plotted in terms of forces (Fig. 9a), strains (Fig. 9b) and stresses (Fig. 9c). The stresses were calculated from the strains as explained in paragraph 3.2 using the initial stiffness moduli and Poisson's ratios obtained on uni-axially loaded beam specimens. However for the load ratio 0/1 for instance, the strain results were non-linear and so the calculated stresses can't be considered as correct.

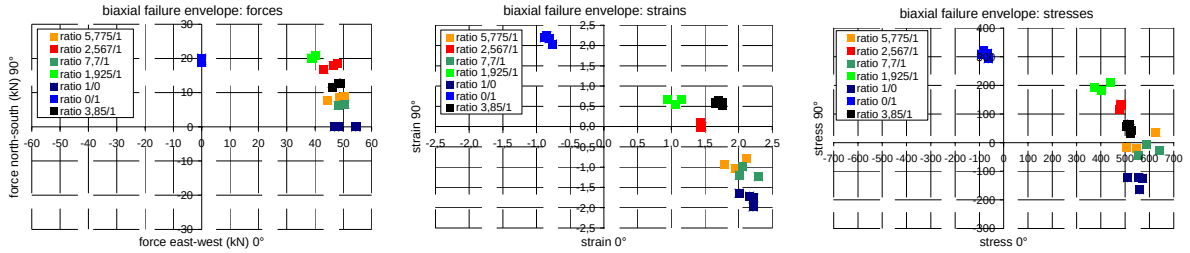

a) forces b) strains c)stresses

Fig. 9. Biaxial failure envelopes for the selected geometry C.

The applied ratio of the forces F_x/F_y is not the same as the ratio of the measured strains $\varepsilon_x/\varepsilon_y$ due to the Poisson effect and is not the same as the ratio of the calculated stresses σ_x/σ_y.

6. DIGITAL IMAGE CORRELATION APPLIED ON THE SELECTED GEOMETRY

After the selection of the cruciform geometry, the digital image correlation technique was used to obtain strain fields for different load ratios. Fig.10 shows the force-strain results for geometry C tested at load ratio 3.85/1. Strains were measured with a strain gage glued at the centre of the specimen's back side both in 0° (x)-, 90° (y)- and 45°- direction. At different load steps, first principal strains obtained with the digital image are shown. The strain values in the middle of the specimen obtained with the digital image correlation technique are comparable to the measured strain values in the 0°-direction, indicated as the blue line on the graph.

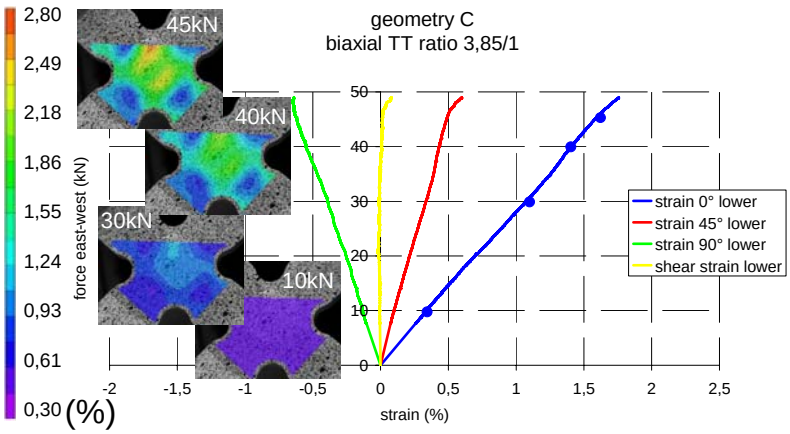

Fig. 10. Digital image correlation and strain gage results for geometry C tested at load ratio 3.85/1.

The same comparison between digital image correlation results and strain gage results was made for different load ratios, giving acceptable agreement.

7. CONCLUSIONS

The combination of finite element simulations and experiments performed on three different geometries of cruciform specimens, led to the selection of a suitable geometry for bi-axial testing of composite materials. This geometry has a reduced thickness in the central region of the specimen, in combination with a rounding radius between two arms inside the material. These features cause failure to occur in the bi-axially loaded test zone, rather than in the uni-axially loaded arms. The digital image correlation technique used for full field strain measurements offers significant advantages over conventional techniques such as strain gauges. The high data point density of the results lead to a better understanding of the behaviour of composites under bi-axial loads. The strain values obtained with the digital image correlation technique are comparable with those measured using strain gauges at the centres of the specimens and with those calculated in the finite element simulations.

ACKNOWLEDGEMENTS

This research is partially funded by the European Commission in the framework of the specific research and technology development programme Energy, Environment and Sustainable Development with contract number ENK6-CT-2001-00552. The authors express their gratitude to LM-Glassfiber in Denmark for producing the cruciform specimens.

BIBLIOGRAPHY

[1] Soden, P. D., Hinton, M. J., Kaddour A. S., “Predicting failure in composite laminates: the background to the exercise”, *Composites Science and Technology*, Vol. 58/7 (1998), pp. 1001-1010.

[2] Soden, P. D., Hinton, M. J., Kaddour, A. S., “A comparison of the predictive capabilities of current failure theories for composite laminates”, *Composites Science and Technology*, Vol. 58/7 (1998), pp. 1225-1254.

[3] Welsh, J. S. and Adams, D. F., “An experimental investigation of the biaxial strength of IM6/3501-6 carbon/epoxy cross-ply laminates using cruciform specimens”, *Composites Part A: Applied Science and Manufacturing*, Vol. 33/6 (2002), pp. 829-839.

[4] Smith, E. W. and Pascoe, K. J., “Biaxial fatigue of a glass-fibre reinforced composite. Part 2: Failure criteria for fatigue and fracture”, *Mechanical Engineering Publications*, London, Appendix 1.

[5] Dawicke, D. S. and Pollock, W. D., “Biaxial testing of 2219-T87 aluminum alloy using cruciform specimens”, *NASA Contractor Report 4782*, (1997).

[6] Tyson J., Schmidt T., Galanulis K., “Advanced photogrammetry for robust deformation and strain measurement”, *accepted for proceedings at SEM 2002 Annual conference*, Milwaukee, WI

[7] Lecompte, D. and Sol, H., *"Digital Image Correlation: A study on the accuracy”*, Internal Report, 2004